

A Variational Edge Partition Model for Supervised Graph Representation Learning

Yilin He¹, Chaojie Wang², Hao Zhang³, Bo Chen⁴, and Mingyuan Zhou¹

¹The University of Texas at Austin, ²Nanyang Technological University

³Cornell University, ⁴Xidian University

February 8, 2022

Abstract

Graph neural networks (GNNs), which propagate the node features through the edges and learn how to transform the aggregated features under label supervision, have achieved great success in supervised feature extraction for both node-level and graph-level classification tasks. However, GNNs typically treat the graph structure as given and ignore how the edges are formed. This paper introduces a graph generative process to model how the observed edges are generated by aggregating the node interactions over a set of overlapping node communities, each of which contributes to the edges via a logical OR mechanism. Based on this generative model, we partition each edge into the summation of multiple community-specific weighted edges, and use them to define community-specific GNNs. A variational inference framework is proposed to jointly learn a GNN based inference network that partitions the edges into different communities, these community-specific GNNs, and a GNN based predictor that combines community-specific GNNs for the end classification task. Extensive evaluations on real-world graph datasets have verified the effectiveness of the proposed method in learning discriminative representations for both node-level and graph-level classification tasks.

1 Introduction

Many real-world entities are bonded by relations, *e.g.*, the users in a social network service are connected by online friendships and the atoms in molecules are held together by chemical bonds. Representing the entities by nodes and relations by edges, a set of interconnected entities naturally forms a graph. Reasoning about these entities and their relations could be conducted under graph neural networks (GNNs) (Atwood & Towsley, 2016; Defferrard et al., 2016; Micheli, 2009; Scarselli et al., 2008). Instead of isolating the feature transformation for each individual entity, GNNs allow the information to be exchanged between related entities. Models employing this strategy have achieved great success in a wide range of applications involving graph structured data, such as classification (Kipf & Welling, 2017; Xu et al., 2019), link prediction (Kipf & Welling, 2016), recommendation (He et al., 2020; Wang et al., 2019), (overlapping) community detection (Mehta et al., 2019; Sun et al., 2019), and drug discovery (Shi et al., 2020).

The essence of many graph-analytic tasks could be summarized as supervised graph representation learning, where the information on the graph is usually characterized by the node features, adjacency matrix, and node or graph labels. A supervised machine learning pipeline is often introduced to embed the nodes or graph under label supervision for a specific classification task. For most of the GNN based methods, the information on nodes and edges are composited through neighborhood

aggregation, *i.e.*, updating the features of each node by combining the features of the surrounding nodes. During this process, the graph structure mostly serves as a given source to indicate the nodes’ neighborhood (Veličković et al., 2018) or provide the weights for aggregation (Kipf & Welling, 2017). Treating the graph structure as given overlooks the latent structures that control the formation of the graph, which, however, could provide valuable information for graph representation learning. In other words, failing to consider the latent graph structures may limit the ultimate potential of this line of work.

One type of latent structure at the hinge of the graph structure and node information is node communities. Their connection to the graph can be explained under a latent-community based graph generation process. For example, both the mixed-membership stochastic blockmodel (MMSB) of Airoldi et al. (2009) and edge partition model (EPM) of Zhou (2015) explain the formation of edges by node interactions over overlapping latent communities. Let us consider person u in social network \mathcal{G} , some of her social connections may be established through interactions with colleagues as a machine learning researcher, some may originate from her interactions with co-members of the same hobby club, and different types of interactions could overlap to strengthen certain social connections between the nodes.

The node community structure also sets the aspects of node information. In the example of social network \mathcal{G} where person u is affiliated with both a research group and a few hobby groups, due to the diverse nature of these different communities, it is likely that she exhibits different characteristics when interacting with co-members of different communities. Namely, the information on u for the research group may be related to her research expertise, and the information on u for the hobby clubs may be related to her hobbies. Therefore, an ideal solution is to learn a different aspect of node properties for each community that it is affiliated with, and represent the overall node information as an aggregation of all community-specific node properties.

Based on this insight, we develop a *variational edge partition model* (VEPM), which is a generative graph representation learning framework. VEPM models how the edges and labels are generated from overlapping latent communities. Instead of hard assigning a node to a single community, VEPM encodes each node into a K -dimensional vector of scores measuring the strength that the node is affiliated with each of the K communities. From these scores we compute the intensities of pairwise interactions within each community. Given that information, under the Bernoulli-Poisson link, the edges could be modeled by the logical OR of independently generated binary latent edges (Zhou, 2015).

The generation of labels includes community-specific node representation learning and aggregation. A key premise of the first part is to detect the hidden structure specified for each community. In our model, it is achieved through edge partition, *i.e.*, decomposing each edge into a summation of link strengths according to the intensities of community-specific interactions. The edge partition step isolates the link strengths accumulated through each community. With the partitioned edges, we learn K separate GNNs to produce community-specific node representations, then compose them into the overall node embeddings to generate the labels. Evaluation shows that the proposed framework can achieve significant performance enhancement on various node and graph classification benchmarks.

We summarize our main contributions as follows:

- We introduce VEPM that utilizes the idea of edge partitioning to extract overlapping latent community structures, which are used to not only enrich node attributes with node-community affiliation scores, but also define community-specific node feature aggregations.
- We formalize the training of VEPM in a variational inference framework, which is powered by GNNs in its latent community inference, representation generation, and label prediction. We further develop an effective pretrain-finetune learning algorithm that exploits the data

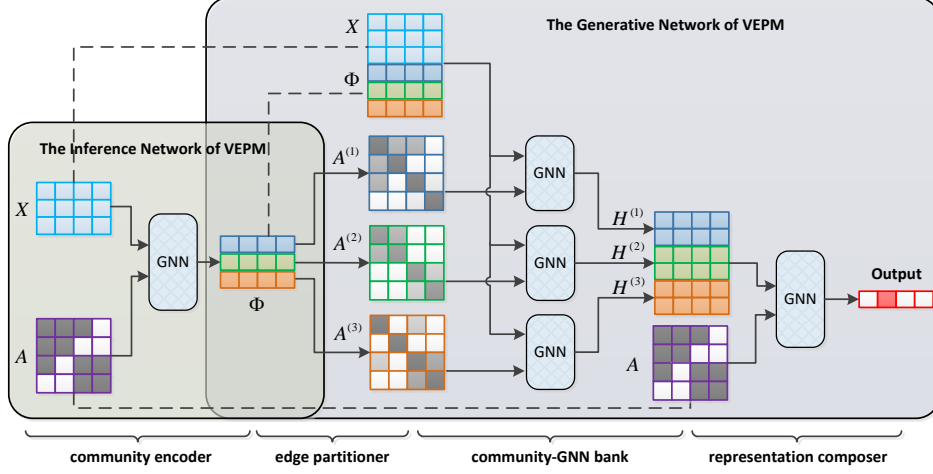


Figure 1: The overview of VEPM’s computation graph. Φ encodes nodes’ affiliation strength to each community, which is used to (1) enrich node features with community information (the dashed line) and (2) partition edges (the solid arrows). The weighted edges obtained from graph partitioning are then passed to an array of independent GNNs to learn community-specific node representations. Finally, they are ensembled to estimate the predictive distribution of the object categories.

generation process.

- We analyze the working mechanism of VEPM and evaluate it over various real-world network datasets. Empirical results show that the proposed VEPM outperforms many previous methods in various node- and graph-level classification tasks.

2 Variational Edge Partition Model

2.1 Preliminaries

The information of a node-attributed graph \mathcal{G} with N nodes could generally be summarized by the dual (\mathbf{X}, \mathbf{A}) , where $\mathbf{X} \in \mathbb{R}^{N \times F}$ is the design matrix whose rows represent node features of dimension F , and \mathbf{A} is an adjacency matrix of shape $N \times N$. The indices of nonzero entries of rows in \mathbf{A} indicate the neighbors of the corresponding nodes, and the values are the initial (unnormalized) edge weights. Structured data numerically expressed in this way could be processed by GNNs, which typically are deep architectures consisting of multiple GNN layers. Let us denote the embedding of node u at the exit of hidden layer l by $\mathbf{h}_u^{(l)}$, the propagation rule of a GNN layer could be summarized as

$$\mathbf{h}_u^{(l)} = \text{agg}\left(f_{\theta}(\mathbf{h}_u^{(l-1)}), \{f_{\theta}(\mathbf{h}_v^{(l-1)})\}_{v \in \mathcal{N}(u)}\right), \quad (1)$$

where $\text{agg}(\cdot)$ is the neighborhood aggregation function, $\mathcal{N}(u)$ denotes the neighbors of u , and $f_{\theta}(\cdot)$ is a transformation function parameterized with θ . Models consisting of GNN layers as described in Equation (1) are collectively referred to as $\text{GNN}_{\theta}(\mathbf{X}, \mathbf{A})$.

Many analytical tasks on node-attributed graphs could boil down to (semi-) supervised classification problems, *i.e.*, given (\mathbf{X}, \mathbf{A}) and observed node or graph labels \mathbf{y}_o , predicting the unobserved labels \mathbf{y}_u ¹. In VEPM, we formalize the classification task as modeling the predictive distribution

¹The unlabeled objects are not limited to node-level, but the prediction task would be based on node-level representations.

as $p(\mathbf{y}_u | \mathbf{X}, \mathbf{A}, \mathbf{y}_o)$, and construct our variational supervised learning pipeline with GNNs as the building blocks.

2.2 Generative task-learning with latent communities

To model $p(\mathbf{y}_u | \mathbf{X}, \mathbf{A}, \mathbf{y}_o)$, we introduce $\Phi \in \mathbb{R}_+^{N \times K}$, a latent positive node-community affiliation matrix, whose entry at the n th row and k th column is interpreted as the strength that the n th node is affiliated with the k th community. Given Φ , we specify a *generative network* as

$$\mathbf{A} \sim p_{\theta}(\mathbf{A} | \Phi), \quad \mathbf{y}_o \sim p_{\theta}(\mathbf{y} | \mathbf{X}, \mathbf{A}, \Phi) \quad (2)$$

to describe how the observed edges \mathbf{A} and labels \mathbf{y}_o are generated. Due to the complexity brought by the deep architecture of the *generative network*, analytically inferring the posterior of Φ is impractical, we hence approximate the posterior $p_{\theta}(\Phi | \mathbf{A}, \mathbf{y}_o)$ with a variational distribution, $q_{\omega}(\Phi | \mathbf{A}, \mathbf{X})$, modeled by a separate GNN based *inference network*. The subscripts θ and ω denote the parameters in the *generative network* and *inference network*, respectively. We illustrate the architectures of both networks in Figure 1. We approximate the posterior predictive distribution using the Monte Carlo method as

$$\hat{p}_{\theta}(\mathbf{y}_u | \mathbf{X}, \mathbf{A}, \mathbf{y}_o) \approx \frac{1}{S} \sum_{s=1}^S p_{\theta}(\mathbf{y}_u | \mathbf{X}, \mathbf{A}, \Phi^{(s)}), \quad (3)$$

where $\Phi^{(s)} \stackrel{iid}{\sim} q_{\omega}(\Phi | \mathbf{A}, \mathbf{X})$ for $s = 1, \dots, S$.

In the remainder of this section, we outline the data generation process and corresponding supportive modules in the *generative network*, introduce the module in the *inference network*, and describe how to train both networks.

2.3 The generation of edges and labels

To model the distribution of the edges given Φ , we adopt the generative process developed in EPM (Zhou, 2015), which explains the generation of the edges under the Bernoulli-Poisson link as $A_{i,j} = \mathbf{1}_{M_{i,j} \geq 1}$, $M_{i,j} \sim \text{Poisson}\left(\sum_{k=1}^K \gamma_k \Phi_{i,k} \Phi_{j,k}\right)$. Here γ_k is a positive community activation level indicator, which measures the member interaction frequency via community k , and in our practice is treated as a trainable parameter amongst θ . We interpret $\gamma_k \Phi_{i,k} \Phi_{j,k}$ as the interaction rate between nodes i and j via community k . The EPM has an alternative representation that partitions each edge into the logical disjunction (*i.e.*, logical OR) of K latent binary edges, expressed as

$$A_{i,j} = \bigvee_{k=1}^K A_{i,j,k}, \quad A_{i,j,k} \sim \text{Ber}(p_{ijk}),$$

where $p_{ijk} := 1 - e^{-\gamma_k \Phi_{i,k} \Phi_{j,k}}$. Thus nodes i and j would be connected as long as their interaction forms up an edge in at least one community. In other words, they are disconnected only if their interactions in all communities fail to generate any edges. Under the EPM, we have the conditional probability as $p_{\theta}(A_{i,j} = 1 | \Phi) = 1 - e^{-\sum_{k=1}^K \gamma_k \Phi_{i,k} \Phi_{j,k}}$. To complete the model, we set the prior distribution of the node-community affiliation matrix as $\Phi \sim \prod_{i=1}^N \prod_{k=1}^K \text{Gam}(\Phi_{i,k}; \alpha, \beta)$.

Given \mathbf{A} and Φ , we now describe the generation process of the labels. The node-community affiliation impacts this process from two aspects: for each node, the corresponding row of Φ serves as side information that could enrich node attributes; for each pair of connected nodes, it could be used to derive the node interactions rate via each community, *i.e.*, $\{\gamma_k \Phi_{i,k} \Phi_{j,k}\}_{k=1,K}$, which are further used to partition the edges to K communities, carried out by the *edge partitioner*:

Edge partitioner. The edge partitioner takes edges \mathbf{A} and node-community affiliation matrix Φ as inputs and returns K positive-weighted edges: $\{\mathbf{A}^{(1)}, \mathbf{A}^{(2)}, \dots, \mathbf{A}^{(K)}\}$, s.t. $\sum_{k=1}^K \mathbf{A}^{(k)} = \mathbf{A}$. The partition function is

$$A_{i,j}^{(k)} = \frac{A_{i,j} \cdot e^{(\gamma_k \Phi_{i,k} \Phi_{j,k})/\tau}}{\sum_{k'} e^{(\gamma_{k'} \Phi_{i,k'} \Phi_{j,k'})/\tau}}, \quad k \in \{1, \dots, K\}, \quad i, j \in \{1, \dots, N\}, \quad (4)$$

where τ is a “temperature” that controls the sharpness of partition.

The values of τ are specified in Table 7 in Appendix C.2. The effect of the *edge partitioner* could be considered as a soft assignment of each edge into different communities. Setting temperature τ to be low could drive the soft assignment towards a hard assignment, and consequently, when aggregating node features with $\{\mathbf{A}^{(1)}, \mathbf{A}^{(2)}, \dots, \mathbf{A}^{(K)}\}$, the edge partitioner would concentrate the information exchange between any two connected nodes at one community. In other words, the mutual influence of the two nodes is relatively high at the community that contributes the most of the interactions between the pair, while being relatively weak at the other communities.

In our implementation, we further generalize Equation (4) to a metacommunity-based edge partition, specifically, by replacing $\gamma_k \Phi_{i,k} \Phi_{j,k}$ with $\Phi_{i,k} \text{diag}(\gamma_k) \Phi'_{j,k}$. In the new expression, $\Phi_{i,k}$ denotes the k th segment in node i ’s community-affiliation encoding, γ_k is a vector of the activation levels for communities in the k th metacommunity. This generalization allows the total number of communities to be greater than K , which enhances the model implementation flexibility at a minor interpretability cost.

The *edge partitioner* provides a soft separation of the information propagation routes for each community, which is passed to the *community-GNN bank* described below for community-specific node representation learning:

Community-GNN bank. The module takes $\mathbf{X}^* := \mathbf{X} \parallel \Phi$ as input², and learns community-specific node embeddings with K separate GNNs, i.e., the outputs are $\mathbf{g}_{\theta}^{(1)}(\mathbf{X}^*)$, $\mathbf{g}_{\theta}^{(2)}(\mathbf{X}^*)$, \dots , $\mathbf{g}_{\theta}^{(K)}(\mathbf{X}^*)$, where

$$\mathbf{g}_{\theta}^{(k)}(\cdot) := \text{GNN}_{\theta}(\cdot, \mathbf{A}^{(k)}), \quad k \in \{1, \dots, K\}.$$

The intention of the *edge partitioner* and *community-GNN bank* is to capture the node information specific to each community. For instance, in a social network, such kind of information could be the different social roles of people when considered affiliated with different social groups, *e.g.*, one may be a former electrical engineering major student in an alumni group, a research scientist in a work group, and an amateur chess player in a hobby club group. As shown in Section 4.5, the node embeddings produced by the *community-GNN bank* are separable by communities.

With the community-specific node embeddings learned by the previous two modules, we finally classify the unlabeled objects by the third module, the *representation composer*:

Representation composer. Let $\mathbf{H}^{(k)} := \mathbf{g}_{\theta}^{(k)}(\mathbf{X}^*)$ denote the node representations learned from the k th community, where $k = 1, \dots, K$, and $f(\cdot)$ denote the representation composer, whose functionality is to project a composite of community-specific node representations to one representation matrix, i.e., $\mathbf{H}_{\mathcal{V}} = f(\mathbf{H}^{(1)}, \mathbf{H}^{(2)}, \dots, \mathbf{H}^{(K)}) := \text{GNN}_{\theta}(\parallel_{k=1}^K \mathbf{H}^{(k)}, \mathbf{A})$. We could further obtain $\mathbf{h}_{\mathcal{G}}$, the vector representation of graph \mathcal{G} , by sending the node level representations $\mathbf{H}_{\mathcal{V}}$ to a graph pooling layer, i.e., $\mathbf{h}_{\mathcal{G}} := \text{GRAPHPOOL}(\mathbf{H}_{\mathcal{V}})$.

²The operator \parallel denotes “concatenation”.

Table 1: Statistics of the datasets used for node- and graph-level classification tasks.

Task	Node Classification			Graph Classification							
Dataset	Cora	Citeseer	Pubmed	IMDB-B	IMDB-M	MUTAG	PTC	NCI1	PROTEINS	RDT-B	RDT-M
Graphs	1	1	1	1000	1500	188	344	4110	1113	2000	5000
Edges	5,429	4,732	44,338	96.5	65.9	19.8	26.0	32.3	72.8	497.7	594.8
Features	1,433	3,703	500	65	59	7	19	37	3	566	734
Nodes	2,708	3,327	19,717	19.8	13.0	17.9	25.5	29.8	39.1	29.6	508.5
Classes	7	6	3	2	3	2	2	2	2	2	5

Taking softmax on the feature dimension of the *representation composer*’s output gives the predicted probabilities of labels, from which we are able to make predictions on the category of the unlabeled objects. Cascading the *edge partitioner* and *community-GNN bank* with the *representation composer* yields the probability $p_{\theta}(\mathbf{y} \mid \mathbf{X}, \mathbf{A}, \Phi)$.

2.4 Variational latent community inference

We use a *community encoder*³ to approximate the posterior distribution $p_{\theta}(\Phi \mid \mathbf{A}, \mathbf{y})$, and provide the *generative network* with the critical latent variable Φ :

Comunity encoder. *The community encoder models the variational posterior $q_{\omega}(\Phi \mid \mathbf{A}, \mathbf{X})$ by a Weibull distribution with shape \mathbf{K} and scale $\mathbf{\Lambda}$, whose parameters are learned by a GNN as $\mathbf{K} \parallel \mathbf{\Lambda} = \text{GNN}_{\omega}(\mathbf{X}, \mathbf{A})$. A Weibull random sample from $q_{\omega}(\Phi \mid \mathbf{A}, \mathbf{X})$ could be created through the inverse CDF transformation of a uniform random variable, given as follows:*

$$\begin{aligned} \Phi &= \mathbf{\Lambda} \odot (-\log(1 - \mathbf{U}))^{\circ(1 \oslash \mathbf{K})}, \\ \mathbf{U}_{i,k} &\stackrel{iid}{\sim} \text{U}(0, 1), \quad \forall (i, k) \in \{1, \dots, N\} \times \{1, \dots, K\}, \end{aligned} \quad (5)$$

where \odot , \oslash , and \circ (in front of superscript⁴) denote element-wise multiplication, division, and power, respectively.

2.5 The overall training algorithm

We train VEPM by optimizing the evidence lower bound (ELBO) as $\mathcal{L} = \mathcal{L}_{\text{task}} + \mathcal{L}_{\text{egen}} + \mathcal{L}_{\text{KL}}$, where

$$\begin{aligned} \mathcal{L}_{\text{task}} &= \mathbb{E}_{q_{\omega}(\Phi)} \log p_{\theta}(\mathbf{y}_o \mid \mathbf{A}, \Phi, \mathbf{X}), \\ \mathcal{L}_{\text{egen}} &= \mathbb{E}_{q_{\omega}(\Phi)} \log p_{\theta}(\mathbf{A} \mid \Phi), \\ \mathcal{L}_{\text{KL}} &= -D_{\text{KL}}(q_{\omega}(\Phi) \parallel p(\Phi)), \end{aligned} \quad (6)$$

where we abbreviate $q_{\omega}(\Phi \mid \mathbf{A}, \mathbf{X})$ with $q_{\omega}(\Phi)$. The three terms in Equation (6) correspond to the classification task, edge generation, and KL-regularization, respectively. Note that our specifications of Φ ’s prior and variational posterior, as in Zhang et al. (2018a), yield an analytical expression of \mathcal{L}_{KL} , as described in detail in Appendix B.

Since modeling the likelihood of the labels involves stacking multiple modules embodied by deep neural networks, approximating the posterior $p_{\theta}(\Phi \mid \mathbf{A}, \mathbf{y}_o)$ is difficult from an optimization perspective. To effectively train VEPM, we leverage the edge generation process and break down

³The *community encoder* is the only module in the *inference network*.

⁴Otherwise, the \circ notation in the context of $f \circ g$ denotes function composition.

the overall training pipeline into two phases: an *unsupervised pretrain*, followed by a *supervised finetune*. In the first phase, we pretrain the *community encoder* until convergence by optimizing $\mathcal{L}_{\text{egen}} + \mathcal{L}_{\text{KL}}$. When it comes to an end, we expect the inferred latent communities to be semantically meaningful to explain the generation of edges.

We then join the pretrained *community encoder* up with the *inference network*, and train the entire architecture with the objective function given in Equation (6). In the second phase, the label supervision is introduced by the additional loss term $\mathcal{L}_{\text{task}}$, which finetunes the latent communities to align them with the end task. To seek better model convergence, in the *supervised finetune* phase, we alternate the training of the *inference network* and *generative network*, i.e., while training one component, we keep the other one fixed. The alternated training scheme allows us to set the steps to train the *inference network* and *generative network* with more flexibility and adapt to each component’s convergence requirement. We summarize the overall training pipeline in Appendix A, and empirically study the effect of specifications in the training algorithm in Section 4.4.

3 Related work

Deep graph generative models: Advances in this line of work include embedding nodes with deep architectures (Kipf & Welling, 2016; Li et al., 2018), and joint optimization with associated graph-analytic tasks such as semi-supervised node classification (Hasanzadeh et al., 2019; Wang et al., 2020) and community discovery (Mehta et al., 2019; Sun et al., 2019). Similar to these models, we regularize the node embeddings Φ by its probabilistic dependency with the graph structure, but instead of simply passing the learned embeddings to a black-box prediction network, we use them to develop a unique label generation process, employing community-specific GNNs for node representation learning and aggregation.

Modeling multi-relational data with GNNs: The topic of handling heterogeneous relational graphs has been extensively studied in the literature of mining Knowledge Graphs (Nickel et al., 2015). With the emergence of GNNs, quite a few attempts (Schlichtkrull et al., 2018; Vashishth et al., 2020) have been made to extend this graph learning paradigm to analytical tasks on multi-relational data. The general idea of adapting GNNs to this type of task is to individually process node representations aggregated from different types of relations, which is similar to our label generation process where information propagation in each community is also individually modeled. However, for most of the instances of this type of application, the feature aggregation paths for different relations are separated either by annotated edge labels, or human-defined “edge types,” whereas in our model, we partition the edges according to node interactions over latent communities, which are inferred from both the observed graph structure and labels from the end task.

Graph factorization based models: Previous works including DisenGCN (Ma et al., 2019) and FactorGCN (Yang et al., 2020) involve factorizing the observed graph and learning representations by combining different graph factors. The motivation of these models is focused on enhancing disentanglement in node representations by learning from “diverse” graph factors. In other words, the expectation of these models on graph factors is on how different they are with each other. These previous factorization based methods purely rely on the label supervision to obtain disentangled latent factors. By contrast, the basis according to which we perform edge partition could be interpreted by communities. We utilize the information from both labels and observed edges to perform edge partitioning and obtain latent factors representing node communities, resulting in a different learning objective and a unique training algorithm.

4 Empirical evaluation

We compare VEPM against a variety of baselines on two common tasks: node classification and graph classification.

4.1 Data preparation

We evaluate VEPM on 11 benchmarks. For node classification, we consider three citation networks: Cora, Citeseer, and Pubmed, which provide bag-of-words document representations as node features and (undirected) citations as edges. For graph classification, we consider four bioinformatics datasets (MUTAG, PTC, NCI1, PROTEINS) and four social network datasets (IMDB-BINARY, IMDB-MULTI, REDDIT-BINARY and REDDIT-MULTI). The input node features are crafted in the same way as Xu et al. (2019). We summarize the statistics of these datasets in Table 1.

4.2 Node classification

Experimental setup: To make a fair comparison, we use the train/test/validation split standardized by the GCNs (Kipf & Welling, 2017) for Cora, Citeseer, and Pubmed. For the *community encoder*, we adopt a similar encoder structure devised by Kipf & Welling (2016), with the nonlinearity set to `softplus`. We select K , the number of metacommunities, through cross-validation, with $K = 4$ for Citeseer and $K = 8$ for Cora and Pubmed. We set the depth of the *generative network* to two layers, and evenly distribute the layers to the *community-GNN bank* and *representation composer*. Specifically, the *community-GNN bank* is implemented with K single-layer GCNs (Kipf & Welling, 2017) and following Veličković et al. (2018), we set their output dimensions as $64/K$. The *representation composer* is implemented with a single-layer GCN (Kipf & Welling, 2017). We record all hyperparameters in Table 7 in Appendix C.2.

Performance comparison: We use classification accuracy as the evaluation metric for node classification. Table 2 reports the average performances of VEPM (\pm standard error) against related baselines that are categorized into three different groups. The first group consists of the GCNs (Kipf & Welling, 2017) and its variant GCN-64 that expands the hidden dimension from 16 to 64. VEPM outperforms the first group by a significant margin. The explanation is twofold: (i) VEPM augments the node attributes with community information carried by the inferred node-community affiliations, (ii) VEPM learns community-specific node embeddings. The second group includes SIG-VAE (Hasanzadeh et al., 2019) and WGCAE (Wang et al., 2020), both of which learn node embeddings from graph generative models jointly optimized with a supervised loss. The performance gain that VEPM obtains could be attributed to our unique label generation process that integrates community information into not only node attributes, but also neighborhood aggregation. The third group (Gao & Ji, 2019; Ma et al., 2019; Veličković et al., 2018) is focused on learning node embeddings leveraging heterogeneous hidden relations. When fitting the hidden relations via attention mechanism, they only use information from the node features through label supervision, whereas our approach also takes the observed graph structure into account via a graph generative model. The additional information from the graph could explain the enhancement achieved by VEPM over the third group.

4.3 Graph classification

Experimental setup: We employ two protocols to evaluate the performance of VEPM on graph classification. Most of the baselines are compared following the 10-fold cross validation based evaluation protocol proposed by Xu et al. (2019). Since this protocol is criticized for being prone to overestimating model performances (Errica et al., 2020), we also evaluate our model following Zhang

Table 2: Comparison of node classification performance. The asterisk (*) marks the results reported by Velićković et al. (2018).

Method	Cora	Citeseer	Pubmed
ChebNet (Defferrard et al., 2016)	81.2	69.8	74.4
GCN (Kipf & Welling, 2017)	81.5	70.3	79.0
GCN-64*	81.4	70.9	79.0
SIG-VAE (Hasanzadeh et al., 2019)	79.7	70.4	79.3
WGCAE (Wang et al., 2020)	82.0	72.1	79.1
GAT* (Velićković et al., 2018)	83.0	72.5	79.0
hGANet (Gao & Ji, 2019)	83.5	<u>72.7</u>	79.2
DisenGCN (Ma et al., 2019)	<u>83.7</u>	73.4	<u>80.5</u>
VEPM (this work)	84.3 \pm 0.1	72.5 \pm 0.1	82.4 \pm 0.2

& Chen (2019), who conduct a more rigorous train-validation-test protocol. For graph classification, we develop VEPM based on both GCN (Kipf & Welling, 2017) and GIN (Xu et al., 2019), and preset the model hyperparameters when evaluating under the first protocol. We provide structural details, the rationale behind hyperparameters determination in Appendix C.1 and sensitivity analysis in Appendix D. Through our studies, we find the variation of VEPM’s graph classification performances with respect to different choices of model architecture or K is quite minor. For the second protocol, we follow the method of Zhang & Chen (2019) to select hyperparameters, and report the test accuracy when the model achieves its highest validation accuracy over 100 epochs of training.

Performance comparison: For the first protocol, we compare VEPM with classical graph classification baselines (Ivanov & Burnaev, 2018; Niepert et al., 2016; Shervashidze et al., 2011), generic-GNN based models (Gao & Ji, 2019; Velićković et al., 2018; Xu et al., 2019), and GNNs with relation-based or task-driven graph factorization (Schlichtkrull et al., 2018; Vashishth et al., 2020; Yang et al., 2020). We could find from Table 3 that VEPM achieves state-of-the-art graph classification performances on 5 out of 8 benchmarks, and the second-best performances on the other 3 benchmarks, among which is the NCI1 dataset, where VEPM outperforms all the other GNN based models.

Table 3: Comparison of graph classification performance (average accuracy \pm standard error).

Method	IMDB-B	IMDB-M	MUTAG	PTC	NCI1	PROTEINS	RDT-B	RDT-M
WL subtree (Shervashidze et al., 2011)	73.8 \pm 3.9	50.9 \pm 3.8	90.4 \pm 5.7	59.9 \pm 4.3	86.0 \pm 1.8	75.0 \pm 3.1	81.0 \pm 3.1	52.5 \pm 2.1
PATCHYSAN (Niepert et al., 2016)	71.0 \pm 2.2	45.2 \pm 2.8	<u>92.6</u> \pm 4.2	60.0 \pm 4.8	78.6 \pm 1.9	75.9 \pm 2.8	86.3 \pm 1.6	49.1 \pm 0.7
AWE (Ivanov & Burnaev, 2018)	74.5 \pm 5.9	51.5 \pm 3.6	87.9 \pm 9.8	-	-	-	87.9 \pm 2.5	54.7 \pm 2.9
GAT (Velićković et al., 2018)	70.5 \pm 2.3	47.8 \pm 3.1	89.4 \pm 6.1	66.7 \pm 5.1	-	-	-	-
hGANet (Gao & Ji, 2019)	-	49.0	90.0	65.0	-	<u>78.7</u>	-	-
GIN (Xu et al., 2019)	75.1 \pm 5.1	<u>52.3</u> \pm 2.8	89.4 \pm 5.6	64.6 \pm 7.0	82.7 \pm 1.6	76.2 \pm 2.8	92.4 \pm 2.5	57.5 \pm 1.5
R-GCN (Schlichtkrull et al., 2018)	-	-	82.3 \pm 9.2	67.8 \pm 13.2	-	-	-	-
CompGCN (Vashishth et al., 2020)	-	-	89.0 \pm 11.1	<u>71.6</u> \pm 12.0	-	-	-	-
FactorGCN (Yang et al., 2020)	<u>75.3</u> \pm 2.7	-	89.9 \pm 6.5	-	-	-	-	-
VEPM (this work)	76.7 \pm 3.1	54.1 \pm 2.1	93.6 \pm 3.4	75.6 \pm 5.9	<u>83.9</u> \pm 1.8	80.5 \pm 2.8	<u>90.5</u> \pm 1.8	<u>55.0</u> \pm 1.5

For the second protocol, aside from a traditional method, WL (Shervashidze et al., 2011), and a generic-GNN based method, DGCNN (Zhang et al., 2018b), we compare VEPM with two GNNs (Verma & Zhang, 2018; Zhang & Chen, 2019) inspired by capsule neural networks (Hinton et al., 2011), which aim to learn different aspects of graph properties via dynamic routing (Sabour et al., 2017). The results in Table 4 show that VEPM outperforms these GNN based methods on most of the benchmarks. This indicates that the aspects of graph information, as defined with communities and learned via aggregating node features with partitioned graphs, are more pertinent to the end

tasks. These empirical results exhibit the efficacy of the proposed latent community-based edge partition model in supervised graph classification.

Table 4: Graph classification accuracy under the second protocol. The baseline results are quoted from Zhang & Chen (2019).

Method	IMDB-B	IMDB-M	MUTAG	NCI1	PROTEINS	RDT-M
WL subtree (Shervashidze et al., 2011)	<u>73.4</u> ± 4.6	49.3 ± 4.8	82.1 ± 0.4	<u>82.2</u> ± 0.2	74.7 ± 0.5	49.4 ± 2.4
DGCNN (Zhang et al., 2018b)	70.0 ± 0.9	47.8 ± 0.9	85.8 ± 1.7	74.4 ± 0.5	75.5 ± 0.9	48.7 ± 4.5
GCAPS-CNN (Verma & Zhang, 2018)	71.7 ± 3.4	48.5 ± 4.1	-	82.7 ± 2.4	<u>76.4</u> ± 4.2	50.1 ± 1.7
CapsGNN (Zhang & Chen, 2019)	73.1 ± 4.8	<u>50.3</u> ± 2.7	<u>86.7</u> ± 6.9	78.4 ± 1.6	76.3 ± 3.6	52.9 ± 1.5
VEPM (this work)	74.6 ± 2.1	50.6 ± 3.6	91.5 ± 4.3	81.7 ± 1.4	76.8 ± 4.1	<u>50.2</u> ± 2.1

4.4 Ablation studies

In this part, we analyze the benefits from three unique designs of VEPM: node attribute augmentation, unsupervised pretraining, and alternated training in the finetune stage.

Various input features: We evaluate the model performance with four types of inputs: random noise, hand-crafted features by Xu et al. (2019), node-community affiliation scores (*i.e.*, Φ), and hand-crafted features augmented with community-affiliation scores. The results are shown in Table 5. The classification accuracy measures the discriminative power of the graph representations learned from these four input types. Comparing the first and second rows with the third row tells us that the inferred node-community affiliation is comparably informative to the end task as hand-crafted node features, both of which are significantly more informative than random noise. We could further conclude by comparing the second row with the fourth row that the information Φ and \mathbf{X} hold for the task enhances the discriminative level of learned representations in a complementary manner. These results verify the quality of Φ as additional node features.

Table 5: Comparison of VEPMs with various input node features.

Random	Hand-crafted	Community-based	IMDB-B	IMDB-M	MUTAG	PTC	NCI1	PROTEINS
✓			64.7 ± 1.6	42.3 ± 1.5	84.6 ± 4.3	63.6 ± 2.0	67.5 ± 2.1	76.5 ± 3.5
	✓		80.3 ± 2.0	53.5 ± 2.6	93.1 ± 5.0	74.7 ± 4.1	68.0 ± 2.1	77.9 ± 2.7
		✓	74.7 ± 5.1	51.5 ± 2.0	84.6 ± 5.5	68.9 ± 3.9	80.8 ± 1.4	75.7 ± 3.8
	✓	✓	76.7 ± 3.1	54.1 ± 2.1	93.6 ± 3.5	75.6 ± 5.9	83.9 ± 1.8	80.5 ± 2.8

Pretraining & alternated training: “Pretraining” and “alternated training” correspond to two elements in our training algorithm: the *unsupervised pretrain* and alternating the training of the *generative network* and *inference network* during the *supervised finetune* stage. In this study, we compare classification results obtained from VEPM trained with both elements (the bottom row in Table 6) against VEPMs trained when at least one of the elements is dropped from the training algorithm (the first 3 rows in Table 6). We could conclude from the results that both pretraining and alternated training contribute significantly to VEPM’s performances.

Table 6: Comparison of VEPMs with various training settings.

Pretraining	Alternated Training	IMDB-B	IMDB-M	MUTAG	PTC	NCI1	PROTEINS
		62.3 ± 5.9	40.3 ± 3.5	74.9 ± 6.5	63.1 ± 6.3	55.0 ± 2.2	65.7 ± 4.3
✓		70.7 ± 1.7	39.0 ± 3.2	90.0 ± 6.3	64.1 ± 2.6	56.0 ± 1.9	70.9 ± 5.1
	✓	61.0 ± 3.6	46.8 ± 0.8	86.6 ± 6.6	68.6 ± 2.0	67.2 ± 8.4	60.6 ± 4.1
✓	✓	76.7 ± 3.1	54.1 ± 2.1	93.6 ± 3.5	75.6 ± 5.9	83.9 ± 1.8	80.5 ± 2.8

4.5 Qualitative analysis

Visualizing community structures: To show that through partitioning the edges, VEPM separates the hidden structure specified for each latent community from the original graph, in Figure 2, we plot the adjacency matrices of 200 nodes from the Cora dataset, before and after edge partition. The 200 nodes are selected via breadth-first search (Moore, 1959) to ensure the connectivity of the sampled subgraph. We sort the nodes sample \mathcal{S} in order to present a clearer view of the community structures. Specifically, we prepare K buckets; for node u , we compute the total interactions it engages under metacommunity k by $\mu_{u,k} := \sum_{v \in \mathcal{S}} \Phi_{u,k} \text{diag}(\gamma_k) \Phi'_{v,k}$, and assign it to bucket k' , where $k' = \arg \max_k \mu_{u,k}$. We first sort the buckets by descending their counts of assigned nodes, then sort the nodes within bucket k , $k \in \{1, \dots, K\}$, by descending value of $\mu_{u,k}$. The Φ used for sorting is sampled at the end of training.

The community structures we detect through the latent community-based graph generative model could be found in Figure 2a as the blocks on the main diagonal. The fact that most of the bright spots (*i.e.*, edges) are located in these on-diagonal blocks reflects dense node connections internal to each community. Sparsely distributed off-diagonal spots provide evidence of overlapping membership between the communities, which is also taken into account by our graph generative model. From Figures 2b to 2i we could see that the *edge partitioner* has done a sound job in separating latent communities. Due to the limited size of the sampled subgraph, not all buckets are assigned with nodes, which causes Figures 2h and 2i to appear empty. To see the effect of edge partition on the entire citation network from the Cora dataset, please refer to Figures 4 to 12 in Appendix E.

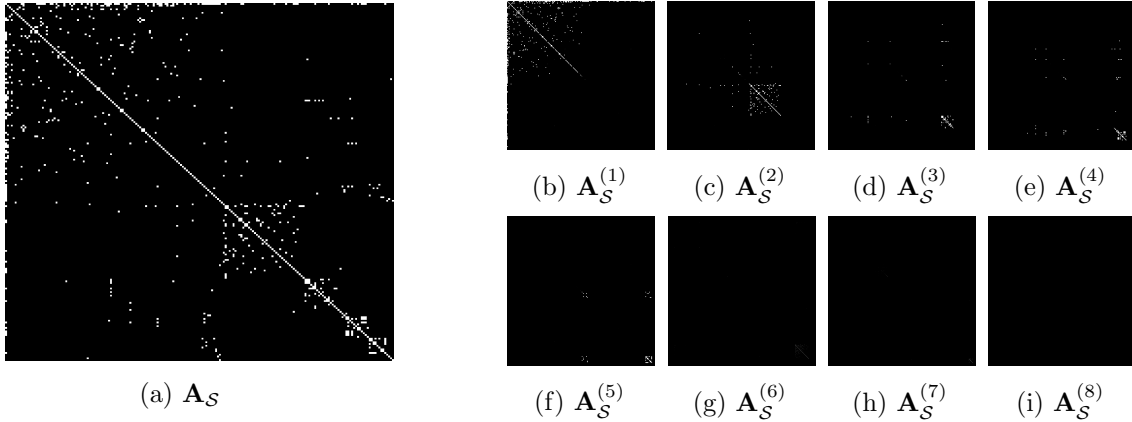


Figure 2: \mathcal{S} is a connected subgraph of 200 nodes sampled from Cora, whose adjacency matrix $\mathbf{A}_{\mathcal{S}}$ is visualized in (a). (b)–(i) shows the results of edge partition, the notation $\mathbf{A}_{\mathcal{S}}^{(k)}$ denotes the k th output from the *edge partitioner*. Brighter color represents larger edge weights.

Visualizing latent representations: The previous visualization experiment verifies that (i) the identified hidden structures are latent communities, and (ii) the partitioned graphs are different from each other. We now study how these propositions contribute to representation learning via visualization. For this experiment, we select Cora as the representative for node classification and MUTAG for graph classification. For the MUTAG dataset, we remove graphs that contain node categories with less than 5 instances (less than 10 from a total of 188) and randomly sample 10 graphs for the visualization experiments.

We first visualize Φ obtained at the end of the *unsupervised pretrain* stage (Figures 3a and 3b), where the 16-dimensional node-community affiliation vectors are projected to 2-D space via t-SNE

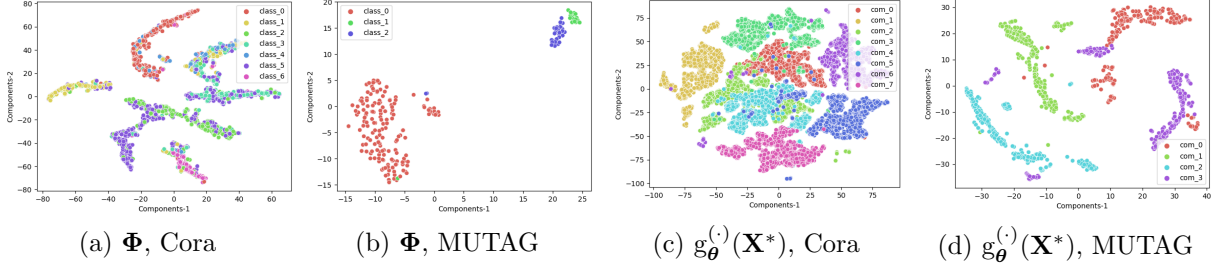


Figure 3: t-SNE visualization of Φ obtained from *unsupervised pretrain* on (a) Cora and (b) MUTAG datasets, as well as community-specific node embeddings obtained during *supervised finetune* on (c) Cora and (d) MUTAG datasets.

(Van der Maaten & Hinton, 2008). The first proposition ensures that the node information carried by these vector representations are about communities. We color code the scatters by node labels, both Figures 3a and 3b exhibit strong correlation between the spatial clusters and colors, which indicates that even without label supervision, the node information provided with Φ has discriminative power on classifying nodes. The finding is compatible with the conclusions in Section 4.4.

We then visualize the community-specific node embeddings obtained at the end of the *supervised finetune* stage (Figures 3c and 3d). Similarly, t-SNE is adopted to reduce the dimensionality of obtained node embeddings. This time we color code the scatters by the latent metacommunity they correspond to. Both Figures 3c and 3d show clear boundaries between the colored clusters, which shows that each community enriches node information from a nonrepetitive angle, potentially enhancing the overall discriminative power of the ensembled node or graph representations and leading to better performance on downstream tasks.

5 Conclusion

Moving beyond treating the graph adjacency matrix as given, we develop variational edge partition models (VEPMs) to extract overlapping node communities and perform community-specific node feature aggregations. Specifically, we first utilize a GNN-based inference network to obtain node-community affiliation strengths, with which we augment node attributes, and partition the edges according to the intensities of node interactions with respect to each community. We learn GNN-based node embeddings for each community by aggregating node features with the corresponding partitioned graph, and aggregate all community-specific node embeddings for the downstream tasks. Extensive qualitative and quantitative experiments on both node-level and graph-level classification tasks are performed to illustrate the working mechanism and demonstrate the efficacy of VEPs in supervised graph representation learning.

References

- Airoldi, E. M., Blei, D., Fienberg, S., and Xing, E. Mixed membership stochastic blockmodels. In *Advances in Neural Information Processing Systems (NeurIPS)*, volume 21, 2009.
- Atwood, J. and Towsley, D. Diffusion-convolutional neural networks. volume 29, 2016.
- Defferrard, M., Bresson, X., and Vandergheynst, P. Convolutional neural networks on graphs with fast localized spectral filtering. In *Advances in Neural Information Processing Systems (NeurIPS)*, volume 29, 2016.

- Errica, F., Podda, M., Bacciu, D., and Micheli, A. A fair comparison of graph neural networks for graph classification. In *International Conference on Learning Representations*, 2020.
- Gao, H. and Ji, S. Graph representation learning via hard and channel-wise attention networks. In *ACM SIGKDD International Conference on Knowledge Discovery & Data Mining (KDD)*, pp. 741–749, 2019.
- Hasanzadeh, A., Hajiramezanali, E., Narayanan, K., Duffield, N., Zhou, M., and Qian, X. Semi-implicit graph variational auto-encoders. In *Advances in Neural Information Processing Systems (NeurIPS)*, volume 32, pp. 10711–10722, 2019.
- He, X., Deng, K., Wang, X., Li, Y., Zhang, Y., and Wang, M. Lightgcn: Simplifying and powering graph convolution network for recommendation. In *Proceedings of the 43rd International ACM SIGIR conference on research and development in Information Retrieval*, pp. 639–648, 2020.
- Hinton, G. E., Krizhevsky, A., and Wang, S. D. Transforming auto-encoders. In *International conference on artificial neural networks*, pp. 44–51. Springer, 2011.
- Ivanov, S. and Burnaev, E. Anonymous walk embeddings. In *International conference on machine learning (ICML)*, pp. 2186–2195, 2018.
- Kipf, T. N. and Welling, M. Variational graph auto-encoders. *arXiv preprint arXiv:1611.07308*, 2016.
- Kipf, T. N. and Welling, M. Semi-supervised classification with graph convolutional networks. In *International Conference on Learning Representations (ICLR)*, 2017.
- Li, Y., Vinyals, O., Dyer, C., Pascanu, R., and Battaglia, P. Learning deep generative models of graphs. *arXiv preprint arXiv:1803.03324*, 2018.
- Ma, J., Cui, P., Kuang, K., Wang, X., and Zhu, W. Disentangled graph convolutional networks. In *International Conference on Machine Learning (ICML)*, pp. 4212–4221, 2019.
- Mehta, N., Carin, L., and Rai, P. Stochastic blockmodels meet graph neural networks. In *International Conference on Machine Learning (ICML)*, pp. 4466–4474, 2019.
- Micheli, A. Neural network for graphs: A contextual constructive approach. *IEEE Transactions on Neural Networks*, 20(3):498–511, 2009.
- Moore, E. F. The shortest path through a maze. In *Proceedings of the International Symposium on the Theory of Switching*, pp. 285–292. Harvard University Press, 1959.
- Nickel, M., Murphy, K., Tresp, V., and Gabrilovich, E. A review of relational machine learning for knowledge graphs. *Proceedings of the IEEE*, 104(1):11–33, 2015.
- Niepert, M., Ahmed, M., and Kutzkov, K. Learning convolutional neural networks for graphs. In *International conference on machine learning (ICML)*, pp. 2014–2023, 2016.
- Sabour, S., Frosst, N., and Hinton, G. E. Dynamic routing between capsules. In *Advances in Neural Information Processing Systems (NeurIPS)*, 2017.
- Scarselli, F., Gori, M., Tsoi, A. C., Hagenbuchner, M., and Monfardini, G. The graph neural network model. *IEEE transactions on neural networks*, 20(1):61–80, 2008.

- Schlichtkrull, M., Kipf, T. N., Bloem, P., Van Den Berg, R., Titov, I., and Welling, M. Modeling relational data with graph convolutional networks. In *European semantic web conference (ESWC)*, pp. 593–607. Springer, 2018.
- Shervashidze, N., Schweitzer, P., Van Leeuwen, E. J., Mehlhorn, K., and Borgwardt, K. M. Weisfeiler-lehman graph kernels. *Journal of Machine Learning Research*, 12(9), 2011.
- Shi, C., Xu, M., Zhu, Z., Zhang, W., Zhang, M., and Tang, J. Graphaf: a flow-based autoregressive model for molecular graph generation. In *International Conference on Learning Representations (ICLR)*, 2020.
- Sun, F.-Y., Qu, M., Hoffmann, J., Huang, C.-W., and Tang, J. vgraph: A generative model for joint community detection and node representation learning. In *Advances in Neural Information Processing Systems (NeurIPS)*, volume 32, 2019.
- Van der Maaten, L. and Hinton, G. Visualizing data using t-sne. *Journal of machine learning research*, 9(11), 2008.
- Vashishth, S., Sanyal, S., Nitin, V., and Talukdar, P. Composition-based multi-relational graph convolutional networks. In *International Conference on Learning Representations (ICLR)*, 2020.
- Veličković, P., Cucurull, G., Casanova, A., Romero, A., Liò, P., and Bengio, Y. Graph attention networks. In *International Conference on Learning Representations (ICLR)*, 2018.
- Verma, S. and Zhang, Z.-L. Graph capsule convolutional neural networks. *arXiv preprint arXiv:1805.08090*, 2018.
- Wang, C., Zhang, H., Chen, B., Wang, D., Wang, Z., and Zhou, M. Deep relational topic modeling via graph poisson gamma belief network. In *Advances in Neural Information Processing Systems (NeurIPS)*, volume 33, 2020.
- Wang, X., He, X., Wang, M., Feng, F., and Chua, T.-S. Neural graph collaborative filtering. In *Proceedings of the 42nd international ACM SIGIR conference on Research and development in Information Retrieval*, pp. 165–174, 2019.
- Xu, K., Hu, W., Leskovec, J., and Jegelka, S. How powerful are graph neural networks? In *International Conference on Learning Representations (ICLR)*, 2019.
- Yang, Y., Feng, Z., Song, M., and Wang, X. Factorizable graph convolutional networks. In *Advances in Neural Information Processing Systems (NeurIPS)*, volume 33, pp. 20286–20296, 2020.
- Zhang, H., Chen, B., Guo, D., and Zhou, M. WHAI: Weibull hybrid autoencoding inference for deep topic modeling. In *International Conference on Learning Representations (ICLR)*, 2018a.
- Zhang, M., Cui, Z., Neumann, M., and Chen, Y. An end-to-end deep learning architecture for graph classification. In *Proceedings of the AAAI Conference on Artificial Intelligence*, volume 32, 2018b.
- Zhang, X. and Chen, L. Capsule graph neural network. In *International Conference on Learning Representations (ICLR)*, 2019.
- Zhou, M. Infinite edge partition models for overlapping community detection and link prediction. In *International Conference on Artificial Intelligence and Statistics (AISTATS)*, volume 38 of *Proceedings of Machine Learning Research*, pp. 1135–1143, 2015.

Appendix

A The pseudocode of training algorithm

Algorithm 1 The overall training algorithm of VEPM

Data: node features \mathbf{X} , observed edges \mathbf{A} , and observed labels \mathbf{y}_o .
Modules: Community ENCoder (CENC), Edge PARTitioner (*EPART), Community-GNN BANK (CGNN_BANK) and REPresentation COMPoser (REPCOMP).
Parameters: ω in the *inference network*, and θ in the *generative network*.
Initialize ω and θ ;
repeat
 $\Phi, \mathbf{K}, \Lambda \leftarrow \text{CENC}(\mathbf{A}, \mathbf{X})$;
 compute $\mathcal{L}_{\text{egen}}$ and \mathcal{L}_{KL} , given in Equation (6);
 $\omega \leftarrow \omega - \eta_{\text{unsup}} \cdot \nabla_{\omega}(\mathcal{L}_{\text{egen}} + \mathcal{L}_{\text{KL}})$;
until CENC converges
repeat
 $\Phi, \mathbf{K}, \Lambda \leftarrow \text{CENC}(\mathbf{A}, \mathbf{X})$;
 $\mathbf{A}^{(1)}, \mathbf{A}^{(2)}, \dots, \mathbf{A}^{(K)} \leftarrow \text{EPART}(\Phi, \mathbf{A})$;
 for $\text{step} \leftarrow 1$ **to** M **do**
 $\hat{\mathbf{y}}_o \leftarrow \text{softmax}(\text{REPCOMP} \circ \text{CGNN_BANK}(\Phi, \mathbf{X}, \mathbf{A}^{(1)}, \mathbf{A}^{(2)}, \dots, \mathbf{A}^{(K)}))$;
 compute $\mathcal{L}_{\text{task}}$, given in Equation (6);
 $\theta \leftarrow \theta - \eta_{\text{sup}, \theta} \cdot \nabla_{\theta} \mathcal{L}_{\text{task}}$;
 end for
 compute \mathcal{L} ;
 $\omega \leftarrow \omega - \eta_{\text{sup}, \omega} \cdot \nabla_{\omega} \mathcal{L}$;
until the whole model converges

B Properties of Weibull distribution

- **Similar density characteristics with gamma distribution**

The Weibull distribution has similar characteristics with the gamma distribution, *i.e.*, the density functions of the two distributions are similar, and both enjoy the flexibility in modeling sparse and nonnegative latent representations.

$$\begin{aligned} \text{Weibull PDF: } P(x|k, \lambda) &= \frac{k}{\lambda^k} x^{k-1} e^{-(x/\lambda)^k}, \\ \text{Gamma PDF: } P(x|\alpha, \beta) &= \frac{\beta^\alpha}{\Gamma(\alpha)} x^{\alpha-1} e^{-\beta x}. \end{aligned} \tag{7}$$

- **Easily Reparameterization**

The latent variable $x \sim \text{Weibull}(k, \lambda)$ can be easily reparameterized as

$$x = \lambda(-\ln(1 - \varepsilon))^{1/k}, \quad \varepsilon \sim \text{Uniform}(0, 1), \tag{8}$$

leading to an expedient and numerically stable gradient calculation.

- **Analytic KL-divergence**

Moverover, the KL-divergence between the Weibull and gamma distributions has an analytic expression formulated as

$$\begin{aligned} \text{KL}(\text{Weibull}(k, \lambda) || \text{Gamma}(\alpha, \beta)) &= -\alpha \ln \lambda + \frac{\gamma \alpha}{k} \\ &+ \ln k + \beta \lambda \Gamma(1 + \frac{1}{k}) - \gamma - 1 - \alpha \ln \beta + \ln \Gamma(\alpha). \end{aligned} \quad (9)$$

C Hyperparameters

C.1 Hyperparameter determination for the graph classification tasks

The model we develop for the graph classification tasks adopt a 2-layer GCN (Kipf & Welling, 2017) for the *community encoder*. The dimension of ϕ is set to 100, and the dimension of the first hidden layer is set to 200 according to the 2:1 ratio in the number of neurons in the first two hidden layers of the GCN based encoder structure which is proved useful in node classification. We implement the *generative network* based on GIN (Xu et al., 2019), which has four consecutive GIN layers whose hidden dimensions are all 64. Similar to our practice in VEPM for node classification, we evenly distribute the 4 layers to the *community-GNN bank* and the *representation composer*; in the *community-GNN bank*, the 64-dimension hidden units are evenly partitioned to all community-specific GNN components. Between the two choices of K we learned from the node classification experiments, we pick the smaller one, *i.e.*, $K = 4$ for the graph classification task, as the sizes of the graphs are much smaller than those for node classification. We conduct sensitivity analyses on the choices of K and the architectures of the *generative network*, and present the results in Appendix D.

C.2 All hyperparameters

D Hyperparameter sensitivity analysis for graph classification

D.1 Number of metacommunities, K

To investigate the sensitivity of VEPM at different choices of K , the number of metacommunities, we hold all other hyperparameters as constants and run 10-fold cross validations with $K \in \{4, 5, 6, 7, 8\}$. From the results in Table 8, we can find that (i) the variation in graph classification performances that VEPM achieves with different values of K is not significant, most of the results recorded in the same column are within one standard deviation with each other; (ii) there is not a collective pattern between model performances and K shared across all benchmarks, in other words, not a single setting of K could consistently outperform other settings on all datasets. Given the above observations, we conclude that the performance of VEPM performances on graph classification is not significantly influenced by the number of metacommunities within a reasonable range.

D.2 Network Structure of the *generative network*

In this part, we focus on studying the potential influence of different network structures on the graph classification tasks. As we decide to make the *generative network* in VEPM to have a comparable amount of parameters with GIN (Xu et al., 2019), the variation space left for the network structure is at how to distribute the 4 GIN layers to the *community-GNN bank* and *representation composer*. We use the name convention VEPM- $\{L_1\}$ - $\{L_2\}$ to denote the variant with L_1 GIN layers in the *community-GNN bank* and L_2 GIN layers in the *representation composer*, where $L_1, L_2 \in \mathbb{Z}_+$ and $L_1 + L_2 = 4$. We hold all other hyperparameters as constants and evaluate VEPM under 3 structures:

Table 7: Hyperparameters settings for VEPM.

Hyperparameters	Experiments	
	Node Classification	Graph Classification
Community ENCoder	Settings	
α	1	1
β	1	1
epoches of <i>unsupervised pretrain</i>	1500	1500
learning rate of <i>unsupervised pretrain</i>	1e-3	1e-2
batch size of <i>unsupervised pretrain</i>	1	32
type of GNN layers	GCN	GCN
module structure	{32}-{16}	{200}-{100}
Edge PARTitioner	Settings	
number of communities	[4,8]	4
the temperature τ for partition	0.1	1
community-GCN bank	Settings	
epoches of jointly training	200	100
learning rate of jointly training	1e-2	1e-3
weight decay of jointly training	5e-4	0.0
batch size of jointly training	1	32
concat weight of Φ	3e-2	3e-4
type of GNN layers	GCN	GIN
module structure	{64}	{64}-{64}
REPresentation COMPoser	Settings	
epoches of jointly training	200	100
learning rate of jointly training	1e-2	1e-3
weight decay of jointly training	5e-4	0.0
batch size of jointly training	1	32
type of GNN layers	GCN	GIN
module structure	{class num}	{64}-{64}-{class num}

VEPM-{1}-{3}, VEPM-{2}-{2} and VEPM-{3}-{1}. From the results shown in Table 9, the graph classification performances that VEPM achieves at different combinations of L_1 and L_2 are quite close to each other, the differences among the results in each column are at low statistical significance level. We hence conclude that the predictive power of VEPM is relatively stable at the variation of the network structure of the *generative network*.

Table 8: Comparisons of VEPs with different numbers of metacommunities. * denotes the value we use in 10-fold cross validation.

Number of metacommunities	IMDB-B	IMDB-M	MUTAG	PTC	NCI1	PROTEINS
4*	76.7 \pm 3.1	54.1 \pm 2.1	93.6 \pm 3.5	75.6 \pm 5.9	83.9 \pm 1.8	80.5 \pm 2.8
5	77.0 \pm 1.8	52.9 \pm 2.2	94.1 \pm 6.3	72.4 \pm 6.5	80.8 \pm 2.2	78.1 \pm 2.3
6	77.3 \pm 3.2	53.9 \pm 2.7	91.5 \pm 6.4	73.5 \pm 5.1	81.0 \pm 3.0	75.8 \pm 2.6
7	77.0 \pm 2.5	54.2 \pm 1.7	94.7 \pm 4.2	71.8 \pm 5.1	82.0 \pm 1.3	79.0 \pm 2.9
8	78.3 \pm 2.1	54.2 \pm 2.1	92.5 \pm 4.3	71.2 \pm 3.7	78.3 \pm 2.9	78.2 \pm 2.9

Table 9: Comparisons of VEPs with various network structures. * denotes the structure we adopt in 10-fold cross validation.

Network Structures	IMDB-B	IMDB-M	MUTAG	PTC	NCI1	PROTEINS
VEPM- $\{1\}$ - $\{3\}$	77.8 \pm 2.0	56.3 \pm 2.1	91.0 \pm 4.9	73.3 \pm 3.6	81.2 \pm 2.5	77.4 \pm 3.6
VEPM- $\{2\}$ - $\{2\}$ *	76.7 \pm 3.1	54.1 \pm 2.1	93.6 \pm 3.5	75.6 \pm 5.9	83.9 \pm 1.8	80.5 \pm 2.8
VEPM- $\{3\}$ - $\{1\}$	74.5 \pm 2.2	54.3 \pm 3.2	87.0 \pm 6.8	66.3 \pm 5.0	84.0 \pm 2.7	78.9 \pm 3.2

E Partitioned Adjacency Matrix

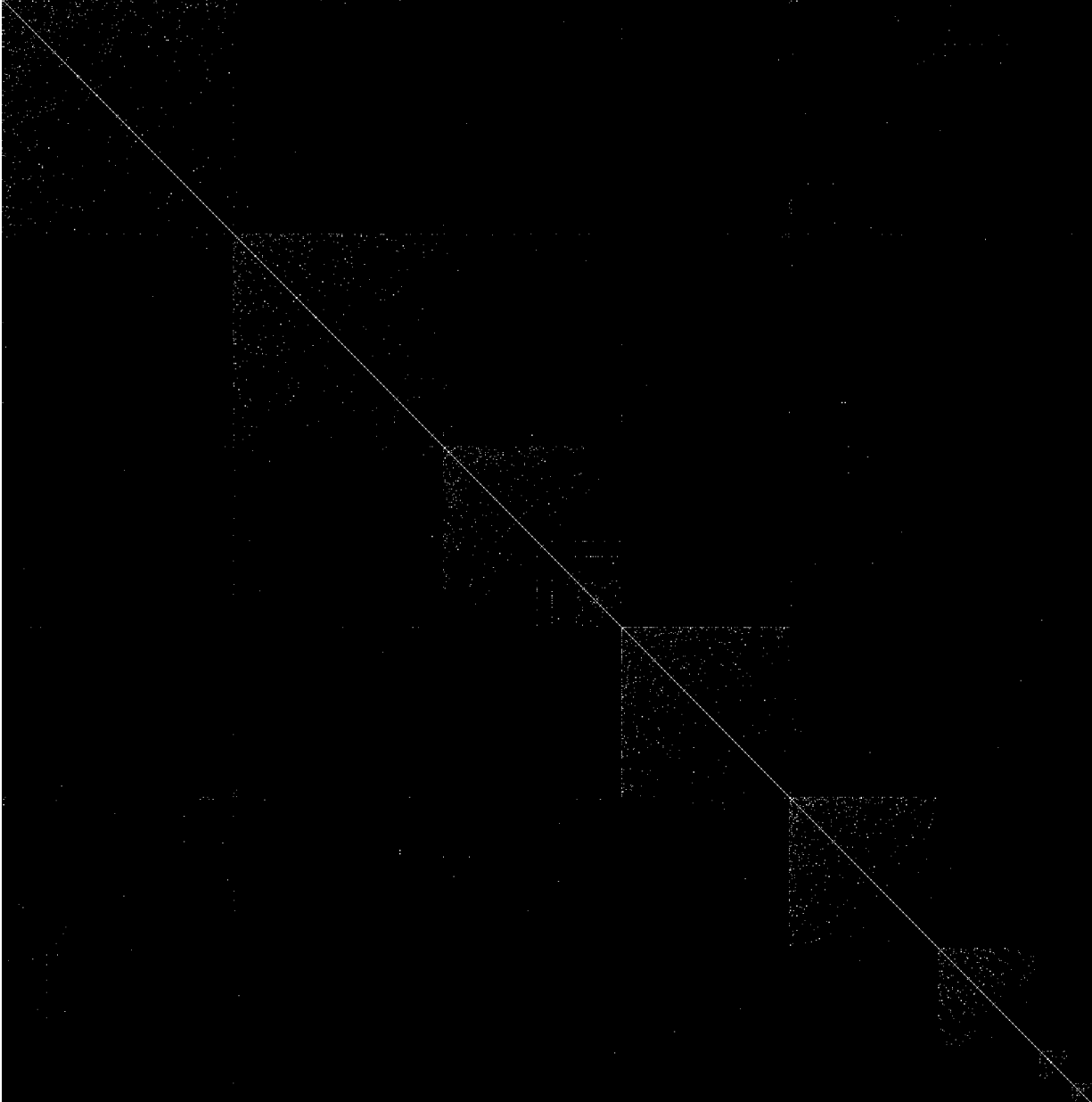


Figure 4: \mathbf{A} , the entire adjacency matrix of the Cora dataset.

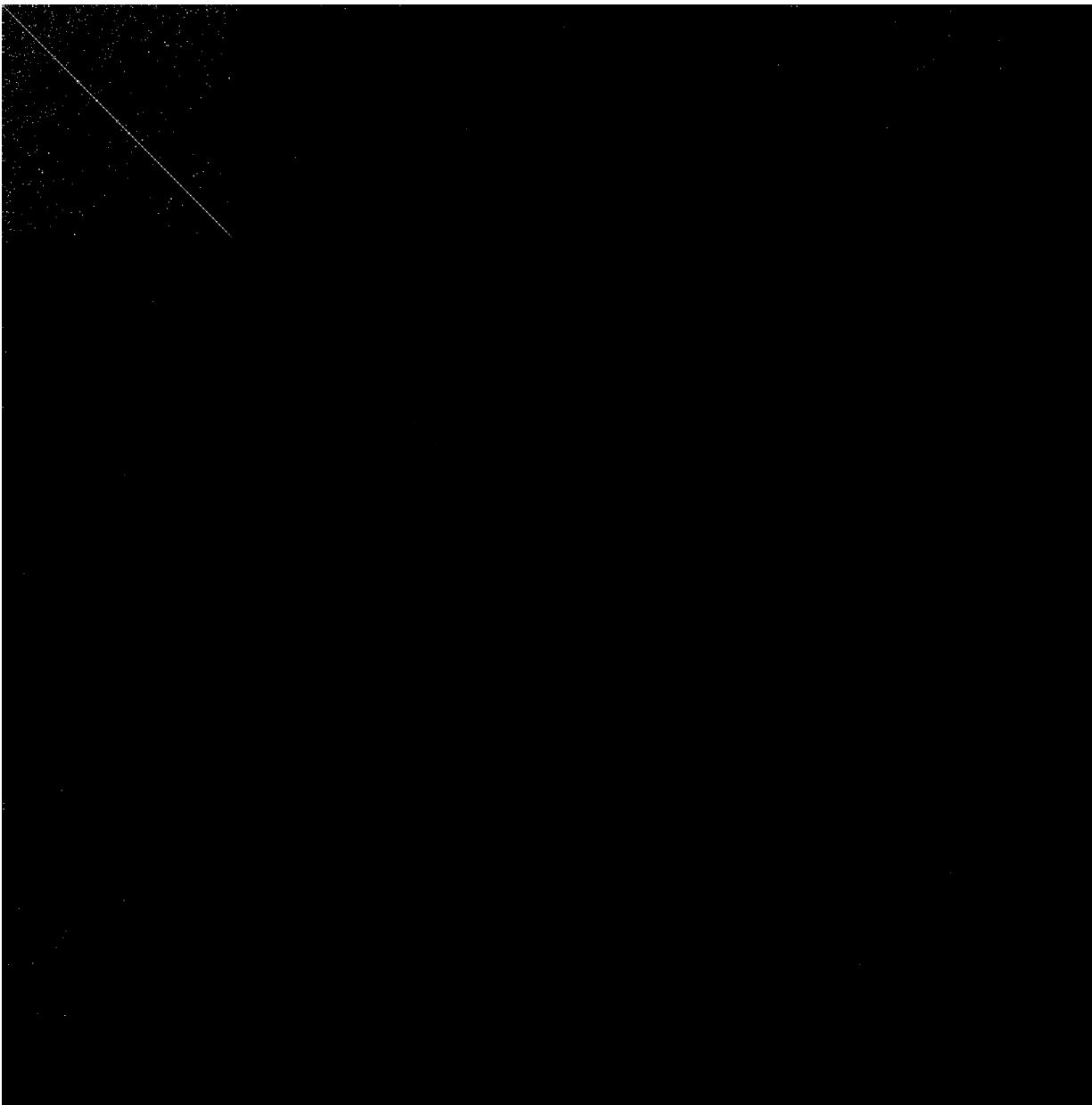


Figure 5: $\mathbf{A}^{(1)}$, the partitioned graph corresponding to the largest metacommunity.

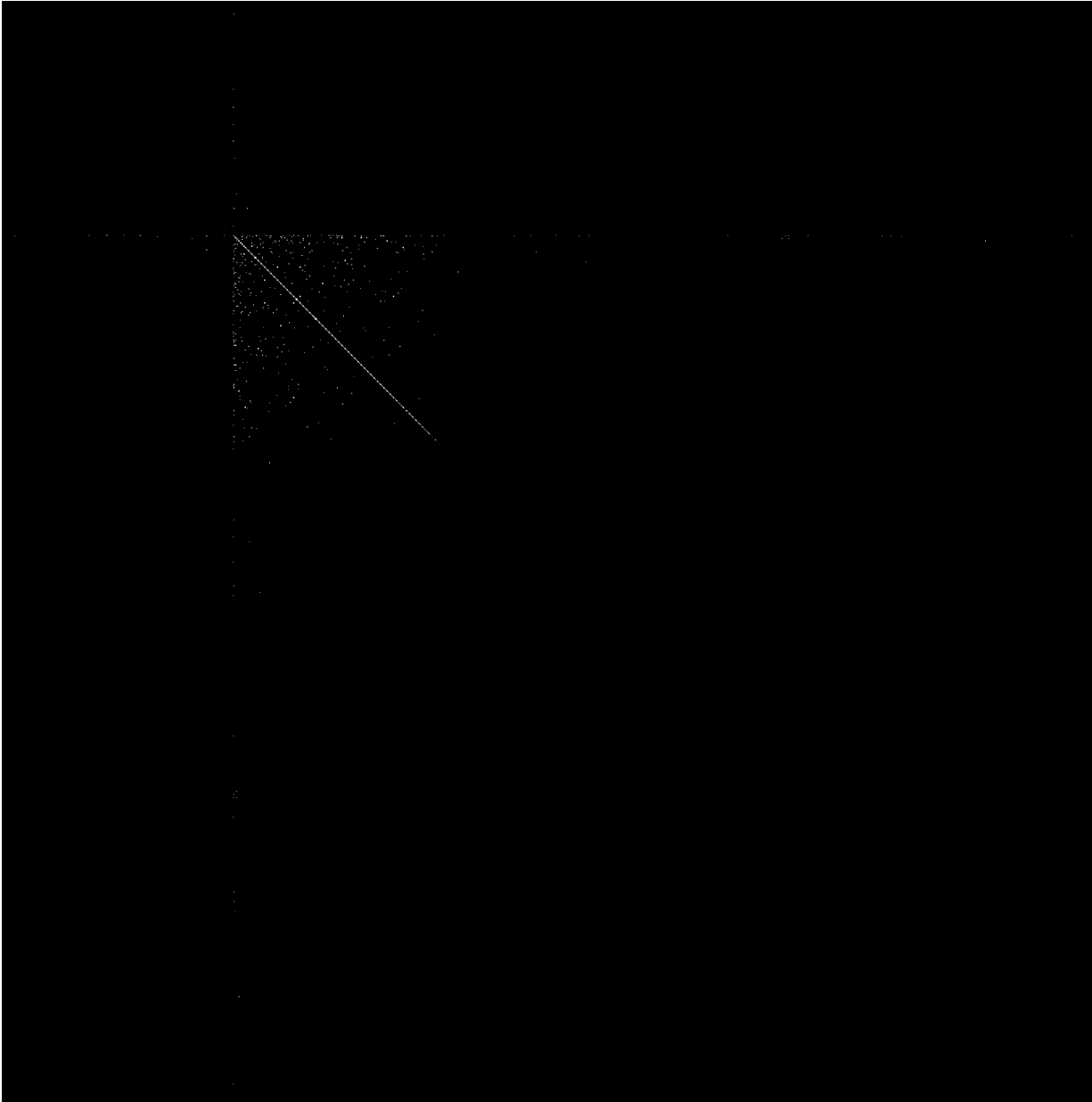


Figure 6: $\mathbf{A}^{(2)}$, the partitioned graph corresponding to the second largest metacommunity.

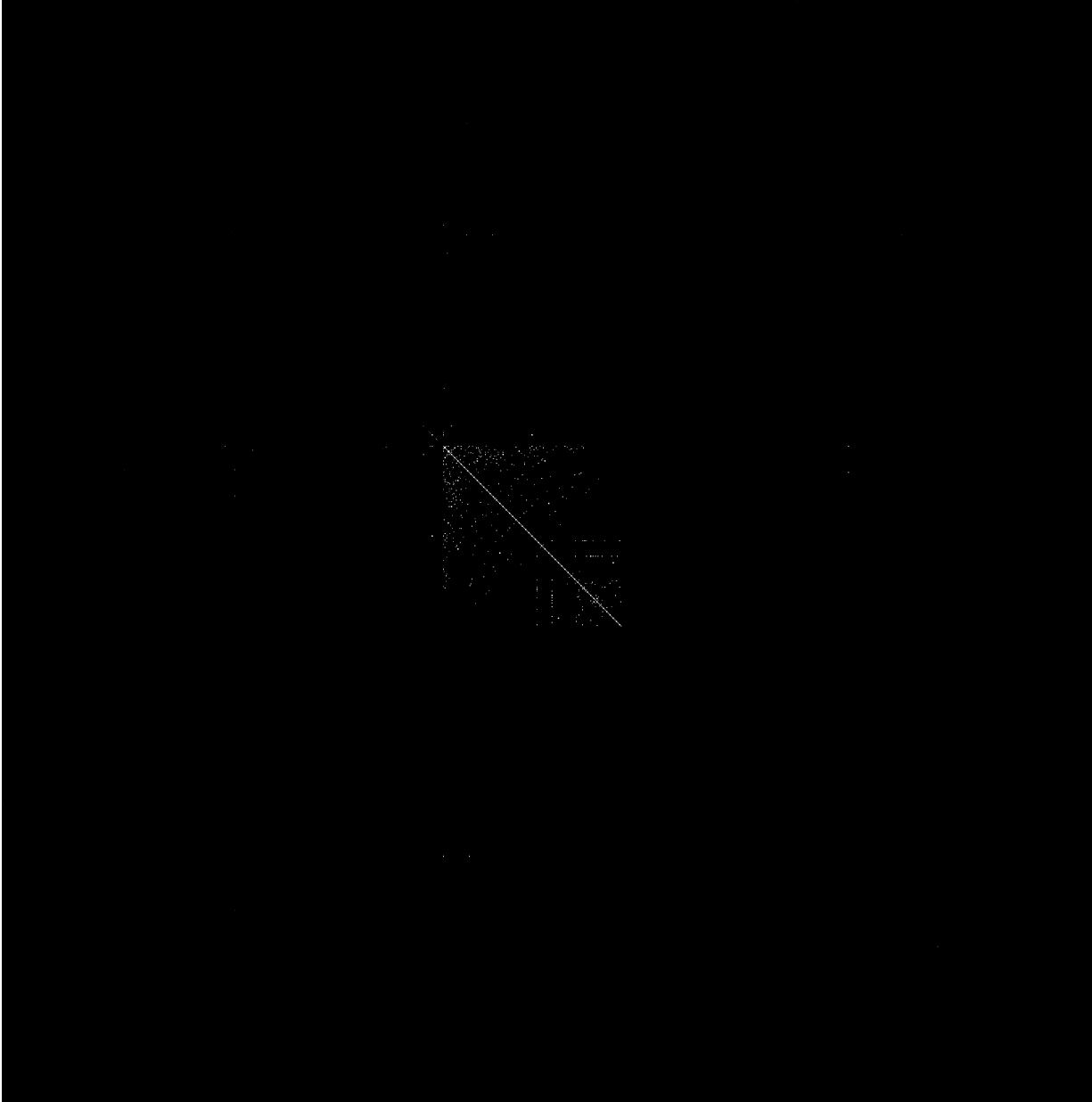


Figure 7: $\mathbf{A}^{(3)}$, the partitioned graph corresponding to the third largest metacommunity.

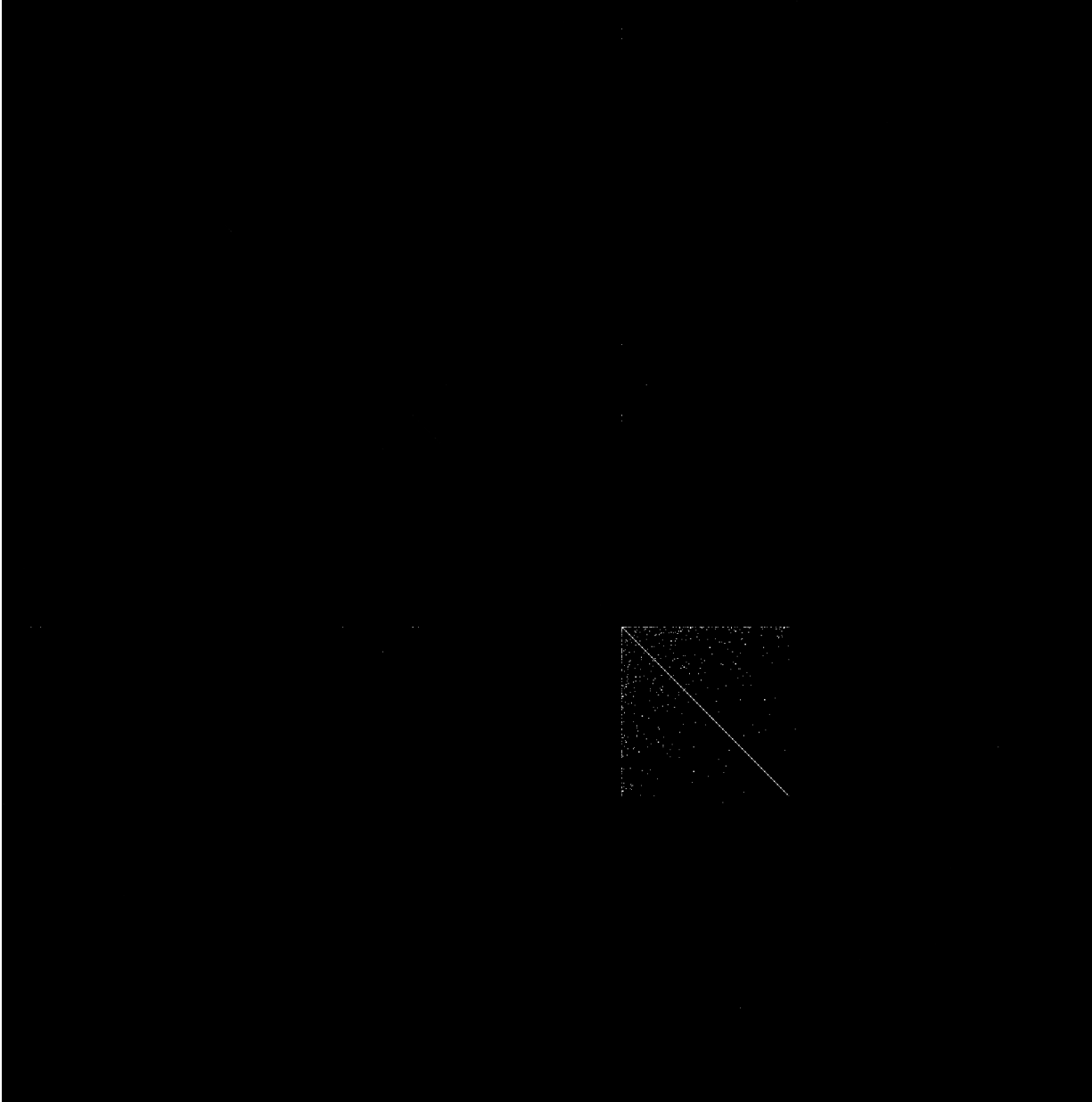


Figure 8: $\mathbf{A}^{(4)}$, the partitioned graph corresponding to the fourth largest metacommunity.

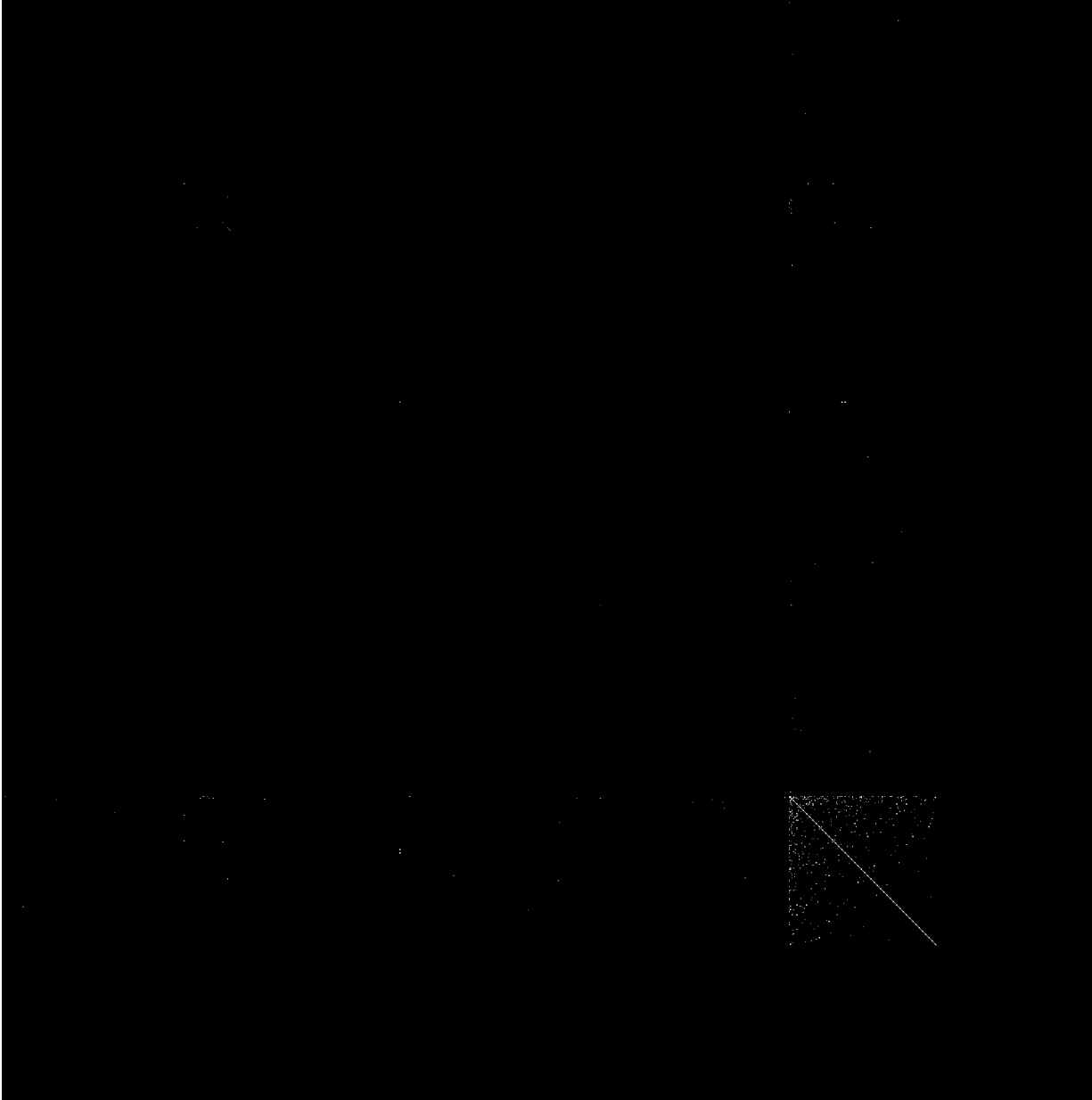


Figure 9: $\mathbf{A}^{(5)}$, the partitioned graph corresponding to the fourth smallest metacommunity.

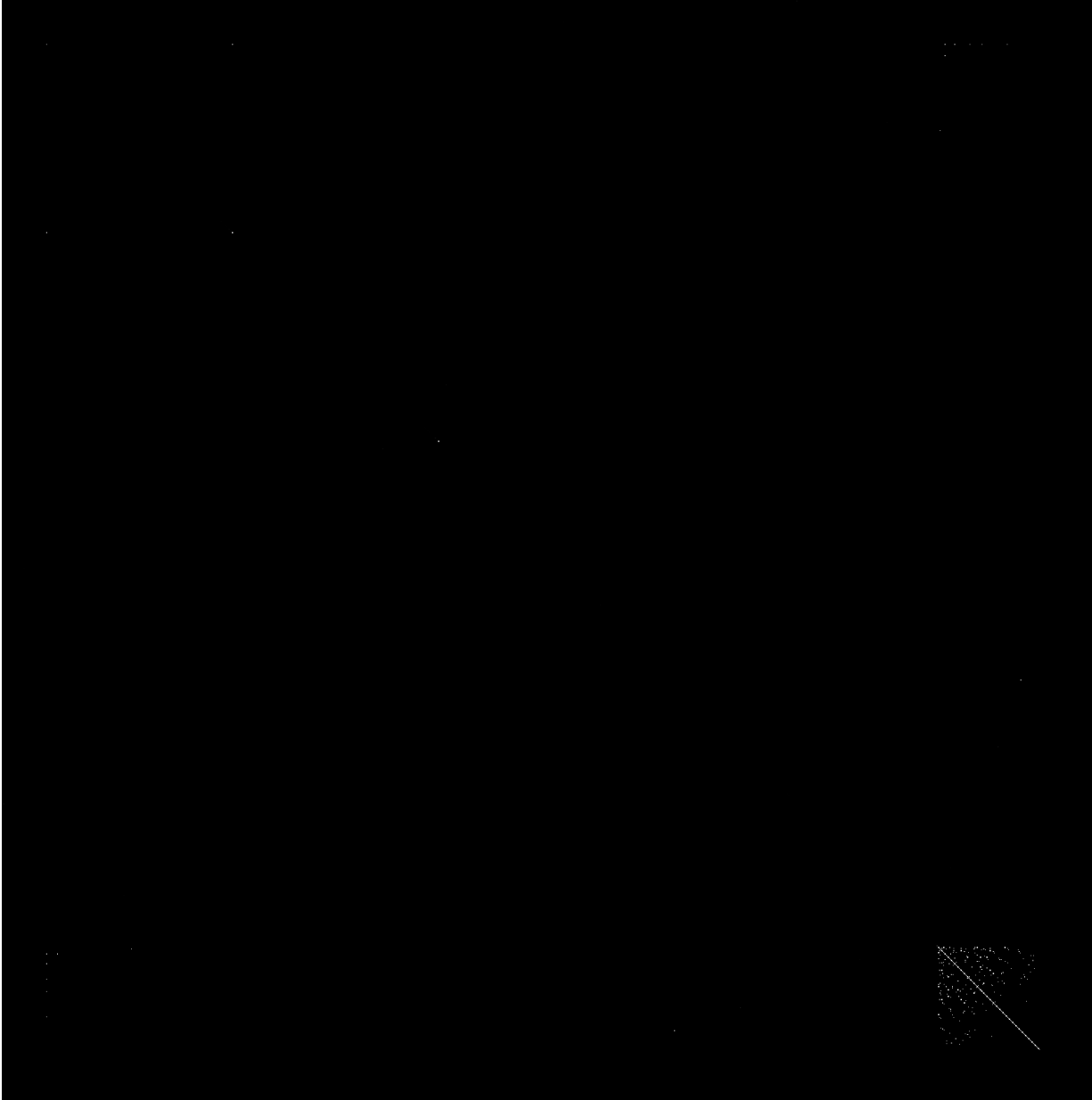


Figure 10: $\mathbf{A}^{(6)}$, the partitioned graph corresponding to the third smallest metacommunity.

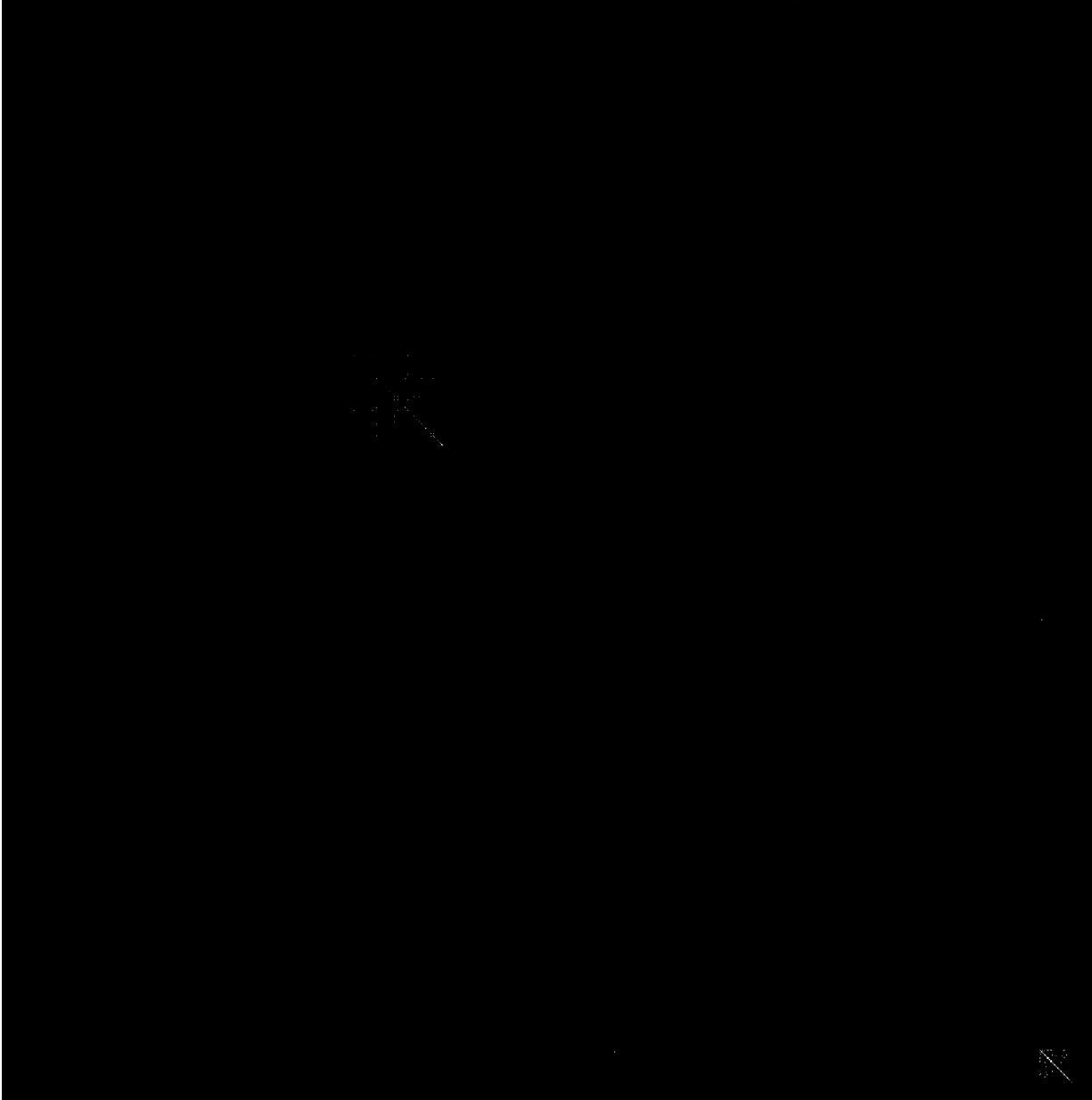


Figure 11: $\mathbf{A}^{(7)}$, the partitioned graph corresponding to the second smallest metacommunity.

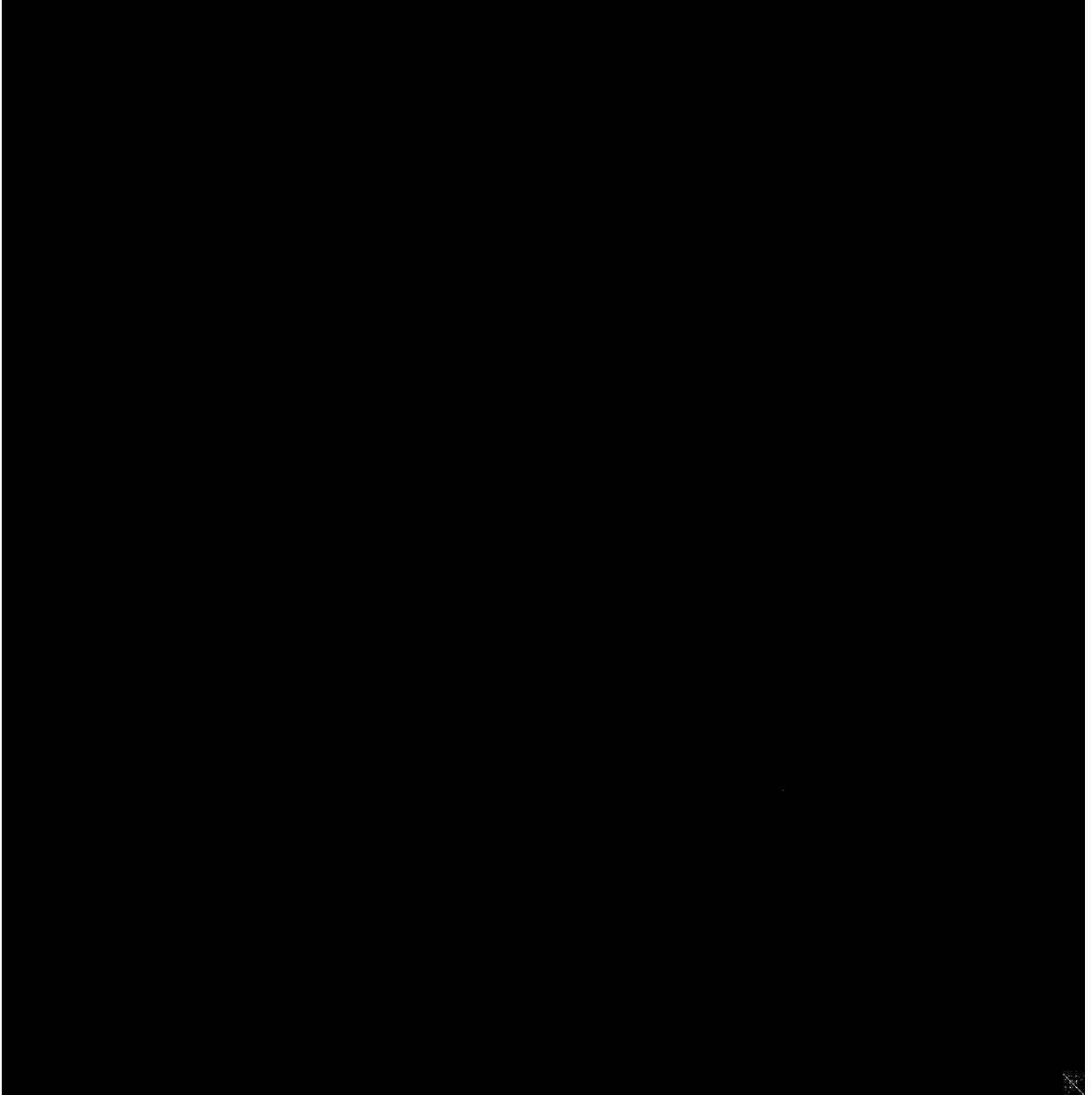


Figure 12: $\mathbf{A}^{(8)}$, the partitioned graph corresponding to the smallest metacommunity.